View Article Online
DOI: 10.1039/C8NJ02131G

Family of [Cu_2], [Cu_4] and [Cu_5] Aggregates: Alteration of Reaction Conditions, Ancillary Bridges and Capping Anions

Manisha Das,[a] Gavin A. Craig,[b] Daniel Escudero,[c] Mark Murrie,[b] Antonio Frontera,[d] and Debashis Ray*[,a]

[a]*Department of Chemistry, Indian Institute of Technology, Kharagpur 721 302, India*

[b]*School of Chemistry, University of Glasgow, Glasgow G12 8QQ, United Kingdom*

[c]*CEISAM UMR CNRS 6230, Université de Nantes, 2 rue de la Houssinière, BP 92208, 44322 Cedex 3 Nantes, France*

[d]*Department of Chemistry, Universitat de les Illes Balears, Crta de Valldemossa km 7.5, 07122 Palma de Mallorca (Baleares), SPAIN.*

View Article Online
DOI: 10.1039/C8NJ02131G

Abstract. Phenoxido-bridged [Cu_2] complex [$Cu_2(\mu–H_4L1)(\mu–OH)(\mu_{1,3}–NO_3)(NO_3)(OH_2)]\cdot H_2O$ (**1**), and its hierarchical [Cu_4] and [Cu_5] assemblies [$Cu_4(\mu–H_4L1)_2(\mu–OH)_2(\mu_{1,3}–ClO_4)(OH_2)_2](ClO_4)_3\cdot 2H_2O$ (**2**), [$Cu_5(\mu–H_4L1)_2(\mu_3–OH)_2(\mu_{1,3}–O_2CCF_3)_2(O_2CCF_3)_2](CF_3COO)_2$ (**3**) were obtained from the reactions of H_5L1 (2,6-bis-{(1,3-dihydroxy-2-methylpropan-2-ylimino)methyl}-4-methylphenol) with three copper(II) salts. Available NO_3^-, ClO_4^- and CF_3COO^- ions have been trapped for 'spontaneous' anion directed 'self-assembly' reactions. All the synthesized complexes contain $[Cu_2(\mu–H_4L1)(\mu–OH)]^{2+}$ fragment, prone to assemble and crystallize [Cu_4] and [Cu_5] complexes in varying reaction conditions. They were characterized by UV–vis and IR spectroscopy, X-ray diffraction analysis and magnetic studies. A change from NO_3^- to ClO_4^- and CF_3COO^- result different course of reaction based on $Cu_2(\mu\text{-}H_4L1)$ fragments. Binding of NO_3^- provided **1** as the isolated [Cu_2] complex by trapping the reactive fragment. In **2** a perchlorate ligand, in $\mu_{1,3}$- binding mode, has been realized as a solitary support for the condensation of two $Cu_2(\mu\text{-}H_4L1)$ fragments. The $\{Cu_5(\mu_3\text{-}OH)_2(\mu_{1,3}\text{-}O_2CCF_3)_2\}^{6+}$ constellation in **3** contains five Cu^{II} centers with a unique Z-in distorted octahedral one in the central position. Binding of different anions to the copper(II) centers controls the nuclearity of the reaction products and tuning of the self-aggregate process within same ligand environment ($\mu\text{-}H_4L1^-$). Magnetic properties of the compounds have been studied both experimentally and using DFT calculations, revealing moderate to strong antiferromagnetic coupling in all aggregates.

View Article Online
DOI: 10.1039/C8NJ02131G

Introduction

In recent years the synthesis, spectroscopic and structural characterization, and catalytic evaluation of Cu_2-compounds have received substantial attention from the view point of their accessibility, structures and their relevance to active sites in biology.[1] For example, the Cu_2 species in tyrosinase is present in a variety of plant and animal tissues.[2] Medicinal Cu^{II} chemistry deals with opportunities in relation to metal ion coordination for the design and use as therapeutic agents that are not attainable through simple organic molecules which are pharmaceutically active.[3,4] In these class of copper(II) complexes the exploitation of the range of coordination numbers and geometries, formation of multinuclear aggregates, thermodynamic and kinetic control, and intrinsic properties of the complex species offer openings for their screening for reactivity patterns and properties. Synthetic endeavor for mimicking Cu enzymes is dependent on the nature and type of the donor atoms available on the ligand backbone. Schiff base ligands are one such type and their Cu^{II} complexes are known to show *in vitro* anticancer potential against the HepG2 cell line.[5] Also Cu_2 compounds of the ligand system are known to promote the hydrolytic cleavage of double-strand plasmid DNA and inhibit the growth of GLC4 and K562 cells without affecting macrophage viability.[6,7]. The presence of phenol unit and adjacent imine functions within ligand frame brings two Cu^{II} (S = ½) centers into close proximity and allows interaction of their electron spins. Available oxygen donors lead to the formation of a Cu_2O_2 type diamond core with modulation from HO^- or O^{2-} bridges, required for further growth in aggregation. The magnetic interaction is subjective to Cu···Cu separation, the Cu−O distances, the Cu−O−Cu angles, the dihedral angle between the planes within the Cu_2O_2 core, the out-of-plane displacement of substituents attached to the bridging groups, and the coordination geometry around each Cu^{II} centre.[1]

Design and synthesis of coordination aggregate complexes, formed by the incorporation of a group of Cu_2-fragments, is dependent on the choice and selection of the ligand system giving ligand anion bound $\{Cu_2L\}$ species in solution. Collapse of two such $\{Cu_2L\}$ fragments provides structurally different $[Cu_4]$ aggregates having cubane,[8] tetrahedron,[9] stepped-cubane,[10] rhomboid,[11] and double-cubane[12] structures. Weak bridges like NO_3^- and ClO_4^- are not appropriate to show similar interactions with $\{Cu_2L\}$ moiety. Whereas carboxylate bridges can adopt $\mu_{1,1}$, $\mu_{1,3}$ or $\mu_{1,1,3}$ modes during such process. Synergistic aggregating potential of HO^- and RCO_2^- groups have been shown to bind $\{Cu_2L\}$ fragments for Cu_6 aggregates.[13]

View Article Online
DOI: 10.1039/C8NJ02131G

From the functional behavior and application point of view the synthesized copper(II) complexes of phenol based multiple alcohol side arm bearing ligand system can be examined for their biomimetic catalytic oxidation efficiency[14] and biophysical studies.[15,16] The hydrogen bonding efficiency and hydrogen bonded network generation in solution from the coordinated and dangling alcohol arms of bound ligand could be useful during association of substrate molecules. In the present work, reactions of H_5L1 (Chart 1, left) have been explored with $Cu(ClO_4)_2$, $Cu(NO_3)_2$ and $Cu(O_2CCF_3)$ to identify the role of anions in directing the assembly process. H_3bemp, a close analog of H_5L1, (Chart 1**,** 2,6-bis-[(2-hydroxy-ethylimino)-methyl]-4-methylphenol; right) is known to give other type of $[Cu_4]$ aggregate.[16] Thus the primary coordinating ability of H_5L1 and *in situ* generated HO^- ions has been judged for aggregation in presence of nitrate, perchlorate and trifluoroacetate ions (Chart S1, ESI). Interestingly three complexes of varying nuclearity has been achieved in $[Cu_2(\mu\text{–}H_4L1)(\mu\text{–}OH)(\mu_{1,3}\text{–}NO_3)(NO_3)(OH_2)]\cdot H_2O$ (**1**), $[Cu_4(\mu\text{–}H_4L1)_2(\mu\text{–}OH)_2(\mu_{1,3}\text{–}ClO_4)(OH_2)_2](ClO_4)_3\cdot 2H_2O$ (**2**) and $[Cu_5(\mu\text{–}H_4L1)_2(\mu_3\text{–}OH)_2(\mu_{1,3}\text{–}O_2CCF_3)_2(O_2CCF_3)_2](CF_3COO)_2$ (**3**). The reproducible synthesis, spectroscopic characterization, molecular structures determination and magnetic properties are described, discoursed and rationalized.

Chart 1 H_5L1 (used in this work) and related H_3bemp

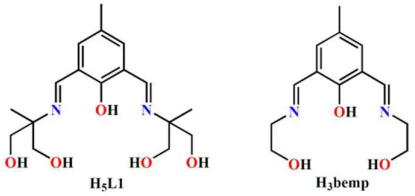

Results and Discussion

Synthetic Protocol

[2,6-bis-{(1,3-dihydroxy-2-methylpropan-2-ylimino)methyl}-4-methylphenol] (H_5L1) was obtained in good yield (Scheme S1, ESI) from a reaction of 2,6-diformyl-4-methylphenol and 2-amino-2-methyl-1,3-propanediol in MeOH under stirring and refluxing condition. Reactions of H_5L1 were examined with different copper(II) salts, as summarized in Scheme 1, to identify the role of anionic groups in directing the self-aggregation processes. Reaction of $Cu(NO_3)_2\cdot 3H_2O$ and H_5L1 in presence of CH_3CO_2Na as base in a 2:1:2 ratio in MeOH-MeCN medium at room temperature stirring condition afforded a greenish solution, from which dark-green crystals of **1** were subsequently isolated in 54% yield. Use of other

View Article Online
DOI: 10.1039/C8NJ02131G

carboxylate salts (propionate, trifluoroacetate) as base did not alter the formation and yield of **1** by incorporating these anions in the molecules. The elemental analysis and single-crystal X-ray diffraction studies confirm the composition of **1** as $[Cu_2(\mu\text{-}H_4L1)(\mu\text{-}OH)(\mu_{1,3}\text{-}NO_3)(NO_3)(OH_2)]\cdot H_2O$.

$$H_5L1 + 2Cu(NO_3)_2\cdot 3H_2O + 2CH_3COONa \xrightarrow{CH_3OH-CH_3CN} [Cu_2(\mu - H_4L1)(\mu - OH)(\mu_{1,3} - NO_3)(NO_3)(OH_2)]\cdot H_2O + 2CH_3COOH + 2NaNO_3 + 3H_2O \quad \cdots(1)$$

Reaction of $Cu(ClO_4)_2\cdot 6H_2O$ with H_5L1 in presence of CH_3CO_2Na in MeOH solution provided a green reaction mixture from which green block shaped crystals of **2** were isolated in 69% yield. Unique bridging coordination of ClO_4^- in presence of available $CH_3CO_2^-$ ions result $[Cu_4]$ complex **2** (eq 2) through a different self-aggregation route without any abound acetate group.

$$2H_5L1 + 4Cu(ClO_4)_2\cdot 6H_2O + 4CH_3COONa \xrightarrow{CH_3OH} [Cu_4(\mu - H_4L1)_2(\mu - OH)_2(\mu_{1,3} - ClO_4)(OH_2)_2](ClO_4)_3\cdot 2H_2O + 4CH_3COOH + 4NaClO_4 + 18H_2O \quad \cdots(2)$$

Reaction of $Cu(CF_3COO)_2\cdot 4H_2O$ and H_5L1 in 2.5:1 molar ratio in stirring MeOH and in absence of any added base, afforded a dark solution, from which **3** (eq 3) was subsequently isolated from the reaction medium as green block shaped single crystals suitable for X-ray analysis in 81% yield.

$$2H_5L1 + 5Cu(CF_3COO)_2\cdot 4H_2O \xrightarrow{CH_3OH} [Cu_5(\mu - H_4L1)_2(\mu_3 - OH)_2(\mu_{1,3} - O_2CCF_3)_2(O_2CCF_3)_2](CF_3COO)_2 + 4CF_3COOH + 18H_2O \quad \cdots(3)$$

The elemental analysis and X-ray diffraction data established the products as $[Cu_4(\mu\text{-}H_4L1)_2(\mu\text{-}OH)_2(\mu_{1,3}\text{-}ClO_4)(OH_2)_2](ClO_4)_3\cdot 2H_2O$ and $[Cu_5(\mu\text{-}H_4L1)_2(\mu_3\text{-}OH)_2(\mu_{1,3}\text{-}O_2CCF_3)_2(O_2CCF_3)_2](CF_3COO)_2$ for **2** and **3** (Scheme 1).

Scheme 1 Synthetic route for **1**–**3**

View Article Online
DOI: 10.1039/C8NJ02131G

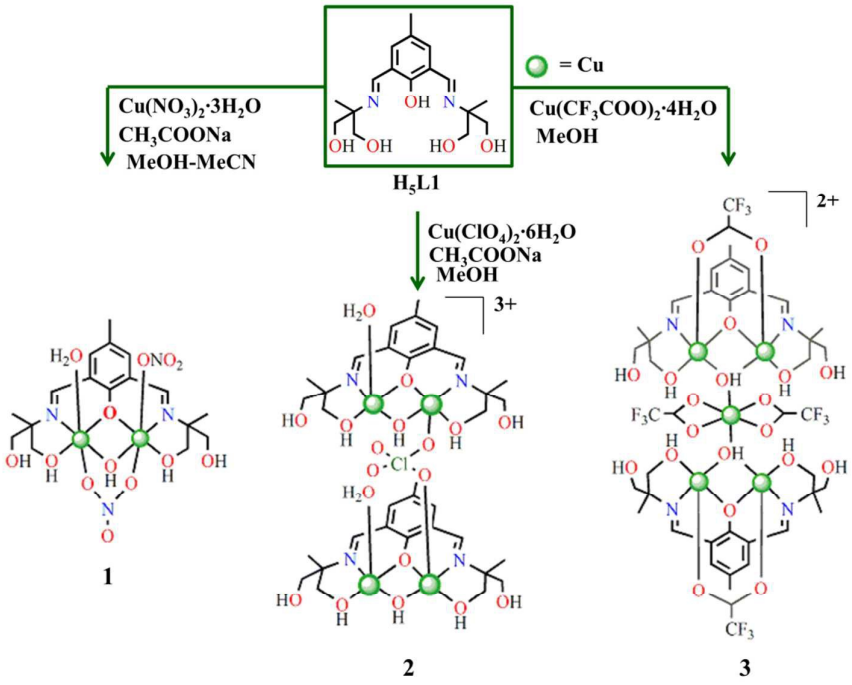

Evaluation by FT-IR Spectroscopy

The FT-IR spectra for **1**, **2** and **3** initially identifies the presence of H_4L1^- in $\{Cu_2(OH)L1\}$ fragments (Figure S1, ESI). The $\bar{\nu}_{C=N}$ stretching frequencies were detected at 1635, 1636 and 1644 cm^{-1} for **1**, **2** and **3** respectively. The phenoxido-bridge shows the $\bar{\nu}_{C-O}$ stretching at 1551, 1560 and 1560 cm^{-1} for **1**, **2** and **3** respectively. Broad bands at 3400 cm^{-1}, 3338 cm^{-1} and 3348 cm^{-1} for **1**, **2**, and **3** respectively were found for alcohol arms and bound hydroxido groups. The coordination of nitrate group in **1** is verified by the presence of the $\nu_3(E')$ mode of vibration at 1384 cm^{-1}.[17,18] Peaks at 1433 cm^{-1} ($\bar{\nu}_{as}$), 1329 cm^{-1}($\bar{\nu}_s$) are assigned to asymmetric and symmetric stretching modes of vibration of the bridging NO_3^- group.[19,20] For complex **2**, the presence of two different types of perchlorate anions have been detected by identifying the characteristic $\bar{\nu}_{as}$ and $\bar{\nu}_s$ stretching vibration modes. For anionic ClO_4^- anions (T_d symmetry), the $\nu_3(T_2)$ (ν_{ClO}) band appeared at ~1088 cm^{-1} and $\nu_4(T_2)$ (δ_{dOClO}) mode at 626 cm^{-1}.[20] In case of bridging (C_{2V}) ClO_4^- anion the ν_3 mode split into three components at 1142, 1111 and 1088 cm^{-1}.[13,21] In **3**, two types of trifluroacetate groups were detected by the presence of broad asymmetric stretching vibrations ($\bar{\nu}_{as(COO)}$) at 1670 cm^{-1} and medium intense symmetric stretching vibrations ($\bar{\nu}_{s(COO)}$) at 1431 and 1329 cm^{-1} respectively. The characteristic $\Delta\bar{\nu}$ value for free $CF_3CO_2^-$group is higher (341 cm^{-1}) compared to the bridged and chelated ones ($\Delta\bar{\nu}$ =239 cm^{-1}).[22,23] The presence of electron withdrawing fluorine atoms moves the asymmetric stretching frequency to higher region.[24]

View Article Online
DOI: 10.1039/C8NJ02131G

Powder X-ray Diffraction Patterns

The powder XRD patterns of the bulk materials of **1-3** were collected using a Bruker AXS X-ray diffractometer and compared with the simulations derived from the single crystal X-ray diffraction data. Figure S2 (ESI) shows that the powder patterns are in good agreement with the simulated data. The difference in intensity is due to the orientation of the powder samples during experiment. The similarity infers that the prepared powder samples are pure and have comparable composition to that of the single crystals. The molecular composition of single crystals and powder samples were same, thus corroborating the reproducibility of powder samples in multiple synthetic attempts.

Electronic Spectral Transitions

In MeOH solutions complexes **1**, **2** and **3** register several characteristic bands within 800-200 nm range. The band maxima at 645 nm (ε = 67 L mol^{-1} cm^{-1}), 666 nm (ε =129 L mol^{-1} cm^{-1}), and 678 nm (ε =104 L mol^{-1} cm^{-1}) are assigned to the low intensity d-d transitions for **1**, **2** and **3**, respectively. The copper(II) centers in octahedral O_6, O_5N and square pyramidal O_4N coordination geometry do register electronic spectral behavior of $[Cu(en)_2(H_2O)_2]^{2+}$ showing corresponding band at 545 nm (ε = 64 L mol^{-1} cm^{-1}).[25] Free ligand H_5L1 in MeOH solution registers n→π* transition at 338 nm (ε = 3600 L mol^{-1} cm^{-1}) and π→π* transition at 232 nm (ε = 18200 L mol^{-1} cm^{-1}). The intense absorptions just below 400 nm are dominated by copper(II) bound ligand-based absorptions. The characteristic phenoxido O to Cu^{II} charge transfer transition (LMCT) is observed at 368 nm (ε = 7600 L mol^{-1} cm^{-1}) for **1**, 374 nm (ε = 10500 L mol^{-1} cm^{-1}) for **2**, and 371 nm (ε_{max} = 13700 L mol^{-1} cm^{-1}) for **3**.[26] Interestingly the other ligand based strong absorption bands were seen at 259 nm with ε values of 3510, 52400 and 64500 L mol^{-1} cm^{-1} for **1**, **2** and **3**, respectively. These are due to Cu^{II} bound intra-ligand π → π* transitions mainly centered on Cu^{II}-bound >C=N functions (Figure S3, ESI).

Description of Crystal Structures

$[Cu_2(\mu\text{-}H_4L1)(\mu\text{-}OH)(\mu_{1,3}\text{-}NO_3)(NO_3)(OH_2)]\cdot H_2O$ (1). X-ray structural analysis shows that **1** crystallized in the monoclinic $P2_1/n$ space group. The interatomic connectivity of the asymmetric unit of **1** is shown in Figure 1, and selected bond distances and angles are given in Table S1 (ESI). The neutral complex is formed from one coordinating Schiff base ligand, two nitrate ions and a lattice water molecule. Two octahedral Cu^{II} centers in the dinuclear unit are bridged by the in plane phenoxido and hydroxido groups resulting in short Cu···Cu separation of 2.896 Å in two adjacent octahedral coordination geometry. Within the Cu_2O_2

View Article Online
DOI: 10.1039/C8NJ02131G

diamond core the Cu–O distances range from 1.910 to 1.958 Å, where the shortest distances are established from phenoxido group. One nitrate group in $\mu_{1,3}$–bridging mode also binds the two copper (II) centers. The O–N–O bridging part of nitrate group connects two almost coplanar CuO_3N planes from two *apical* sides and register a dihedral angle of 5.68°.

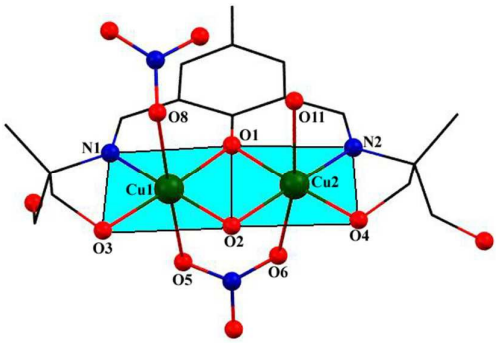

Figure 1 Molecular view of **1** with partial atom numbering scheme. H-atoms are omitted for clarity. Color code: Cu, green, N, blue, O, red, C, black

The N_2O_5 donors of H_5L1 provided two phenoxido-bridged *meridional* O_2N halves to bind two Cu^{II} centers. The second $–CH_2OH$ arms on each side remain pendant and participate in hydrogen bonding interactions within the crystal lattice. For NO_5 octahedral geometry, the Cu–N and Cu–O distances range from 1.927 to 2.475 Å for Cu1 and 1.910 to 2.574 Å for Cu2 centers respectively. Cu–O bond from bridging nitrate provides the longest (2.574 Å) separation above the CuO_3N plane (for Cu1 center). The other Cu–O bond distance (for Cu2 center) from bridging nitrate is 2.432 Å, confirming the asymmetric bridging by NO_3^- group. The water O atom is found at 2.549 Å from Cu2, whereas the O atom of the NO_3^- group is at 2.475 Å from Cu1.

Two discrete molecular units are engaged in intermolecular hydrogen bonding interactions involving the coordinated hydroxyl group of a ligand arm with a hydroxide bridge (O4–H4···O2) and dangling hydroxide group (O3–H3···O12), producing a hydrogen bonded dimeric assembly of two Cu_2 units. The coordinated water molecule functions both as a hydrogen bond donor and acceptor and form hydrogen bonding interactions with the nitrate ion (O11–H11B···O7, O11–H11A···O9) and lattice trapped water molecule (O1W–H1WA···O11). The lattice water molecule also involved in hydrogen bonding interaction with available nitrate (O1W–H1WB···O7), bridging hydroxide (O2–H2···O1W) and dangling hydroxyl group of ligand (O12–H12···O1W). Such hydrogen-bonding interactions extend the hydrogen bonded dimeric assembly in two dimensions producing a two dimensional hydrogen bonded network (Figure 2).

View Article Online
DOI: 10.1039/C8NJ02131G

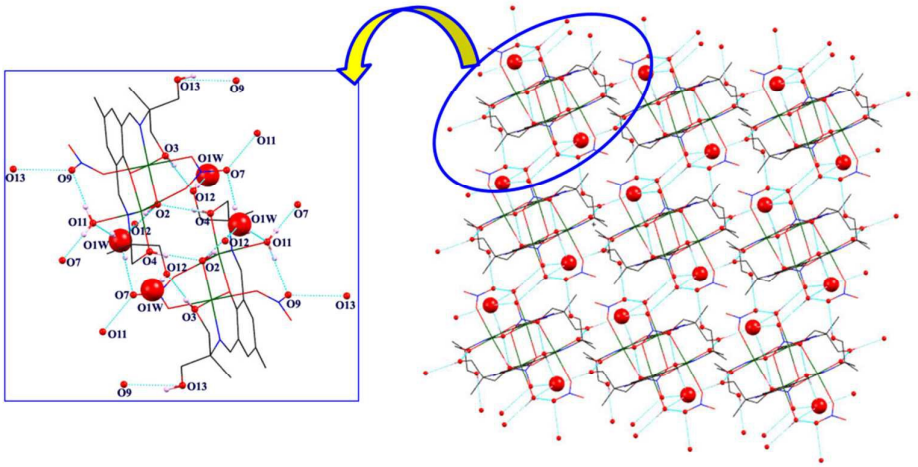

Figure 2 Hydrogen bonded 2D network in **1**; inset: hydrogen bonded dimeric units

$[Cu_4(\mu\text{-}H_4L1)_2(\mu\text{–}OH)_2(\mu_{1,3}\text{-}ClO_4)(OH_2)_2](ClO_4)_3\cdot 2H_2O$ (2). The structure of the tetranuclear Cu^{II} complex is shown in Figure 3. Selected interatomic distances and bond angles are provided in Table S1 (ESI). It crystallizes in the triclinic $P\bar{1}$ space group and consists of a tricationic $[Cu_4(\mu\text{-}H_4L1)_2(\mu\text{–}OH)_2(\mu_{1,3}\text{-}ClO_4)(OH_2)_2]$ part and three ClO_4^- anions. X-ray diffraction quality single crystals were obtained as perchlorate salts.

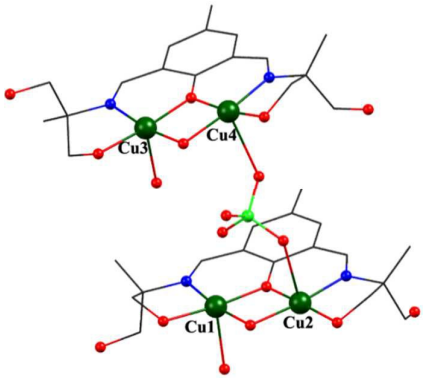

Figure 3 Molecular view of cationic part of **2** with partial atom numbering scheme. H-atoms and counter anions are omitted for clarity. Color code: Cu, green, N, blue, O, red, Cl, olive, C, black

Anionic H_4L1^- each providing a N_2O_5 donor set is suitable to provide the Cu_4 complex with unique bridging mode of a perchlorate anion. Unlike complex **1**, all the Cu^{II} centers are in square pyramidal geometry well suited for lone inter-dimeric bridging support from one ClO_4^- ion. Each H_4L1^- unit provides basal coordination support to two Cu^{II} ions which are tightly bridged by hydroxido O atom within the same plane. Herein all four Cu^{II} ions are in NO_4 square pyramidal geometry and the Cu–N and Cu–O distances range from 1.912 to 2.638 Å. Cu–O bond distances from bound water molecules are 2.354 and 2.357 Å,[27] whereas Cu–O bonds from bridging perchlorate ($\mu_{1,3}$-ClO_4^-) O atoms give longest (2.584 Å for Cu4

View Article Online
DOI: 10.1039/C8NJ02131G

and 2.638 Å for Cu2) Cu–O bonds below and above the two CuO_3N square planes. Very weak coordination of these O atoms shows only *square-pyramidal* environment around each metal ion. As a result the Addison parameter τ remains in the 0.007−0.055 range (Figure 4).[28]

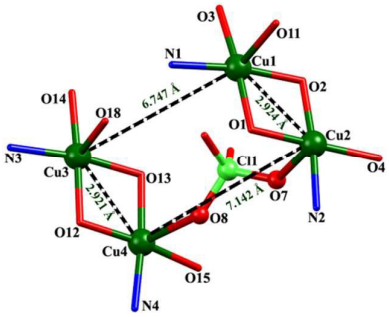

Figure 4 Core view of cationic part of **2** showing up down *apical* coordination relative to the *basal* planes

The metallic core of **2** resulting from the perchlorate−mediated assembly takes the shape of a trapezium (Figure 4). Perchlorato bridged Cu^{II} centers (Cu···Cu) are 7.142 Å apart compared to the phenoxido-hydroxido bridged separation of 2.921 Å. The open side registers a Cu···Cu separation of 6.747Å. The presence of two water molecules in **2** shows hydrogen bonding network with dangling ligand alcohol arms.

For **2** the coordinated hydroxyl group of ligand arm was involved in intermolecular hydrogen-bonding interactions with dangling hydroxyl group (O4–H4···O16) and with bridging –OH group (O3–H3···O13, O14–H14···O2). Hydrogen bonding interactions of the dangling hydroxyl groups with each other (O6–H6···O17) and with lattice water molecule (O5–H5···O1W, O16–H16···O1W) are also observed. The bridging hydroxyl group and coordinated water molecule remain involved in intramolecular hydrogen-bonding interactions with bridging perchlorate (O13–H13···O10, O18–H18B···O9). Hydrogen bonding interactions are also observed between coordinated water molecule and perchlorate counter anion (O18–H18A···O21) as well as dangling –OH group and perchlorate counter anion (O17–H17···O30). Further expansion through hydrogen bonding interactions occur via lattice water molecules (O1W–H1WA···O22, O2W–H2WA···O30, O2W–H2WB···O5, O1W–H1WB···O26, O15–H15···O2W) producing a 2D sheet structure (Figure 5). These non-covalent and non-bonding interactions play an important role in the crystal lattice with entrapment of anions and lattice solvent molecules.

View Article Online
DOI: 10.1039/C8NJ02131G

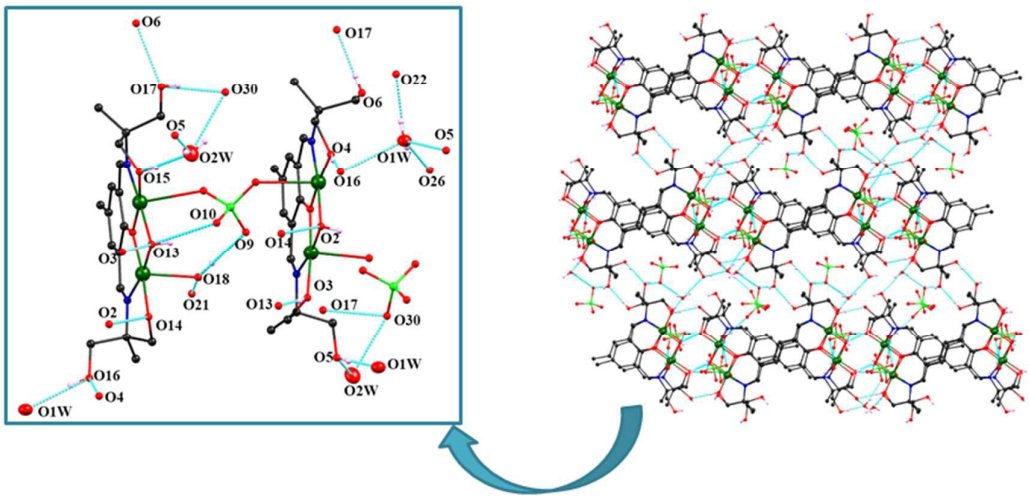

Figure 5 Supramolecular supports from hydrogen bonding in **2**

$[Cu_5(\mu\text{-}H_4L1)_2(\mu_3\text{-}OH)_2(\mu_{1,3}\text{-}O_2CCF_3)_2(O_2CCF_3)_2](CF_3COO)_2$ (3). Complex **3** crystallizes in the monoclinic $P2_1/c$ space group with Z=2 and crystallographic inversion center on Cu3 atom. The selected metric parameters for the structure are summarized in Table S1 (ESI). The asymmetric unit of **3** contains half of the molecular structure and one trifluroacetate counter anion. A centrosymmetric structure containing five Cu^{II} centers within a $[Cu_5O_4]$ core generates through intermetallic connections from H_4L1^- and water derived HO^- anions. Four trifluroacetate groups connect the ligand bound Cu^{II} centers and coordinate to the central Cu^{II} ion in bidentate fashion (Figure 6).

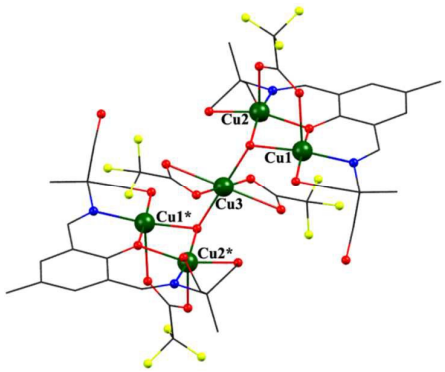

Figure 6 Molecular view of cationic part of **3** with partial atom numbering scheme. H atoms and counter anions are omitted for clarity. Color code: Cu, green; N, blue; O, red; F, lemon green; C, black

Within the $Cu_2(\mu\text{-}H_4L1)$ fragments two square pyramidal Cu^{II} centers are connected by the in plane phenoxido and hydroxido groups and bringing the Cu^{II} centers at a distance of 2.909 Å. The square pyramidal natures of these Cu^{II} centers are known from the calculated Addison parameters (τ) of 0.01 and 0.12. The Cu–O distances within this Cu_2O_2 diamond core range

View Article Online
DOI: 10.1039/C8NJ02131G

from 1.924 to 1.995 Å. Interestingly the central Cu3 is a unique one and adopts a typical O_6 octahedral coordination geometry. The environment is developed from forced bidentate coordination of two trifluroacetato (O7, O8, O7* and O8*) groups in a *basal* plane. The corresponding Cu–O bond distances were longer in 1.976−2.048 Å range and characteristic with four long distances in case of copper(II) ion in octahedral geometry and susceptible to Jahn-Teller distortion. Two *apical* positions around this central Cu atom are occupied by the μ_3–OH group providing two short Cu3−O2 bonds of 1.919 Å separations, clearly demonstrating an unusual example of a compressed coordination octahedron within a [Cu_5] compound (Figure 7c).

Two such μ_3–OH bridges provide lone supports to the central copper(II) for aggregation. For such bridge two types of Cu–O_{OH} bond distances are observed, the smaller (1.919 Å) ones connect the Cu3 and longer ones (1.975 and 1.995 Å) are present within Cu_2(μ-H_4L1) fragments. In one of our previous work we have shown that the affinity of the copper(II) ions for long distance binding along the *apical* Jahn-Teller axis is responsible for the binding of six acetate ions,[29] unlike the fluoroacetate anions in the present work, in three different coordination modes. The central copper(II) ion adopts a compressed octahedral geometry owing to the compression in *apical* direction, with a significant compression of the *apical* bonds by 0.093 Å, when compared by considering six Cu–O bonds around Cu3. In the present case the forced coordination from two alcohol side arms and availability of mononuclear copper(II)trifluoroacetate fragment in the reaction medium are responsible for the formation of the different type of [Cu_5] coordination aggregate.[29,30] Two other trifluroacetate groups binding Cu1 (Cu1*) and Cu2 (Cu2*) in $\mu_{1,3}$ bridging mode pushes the ligand bound Cu_2 fragments to entrap the central copper(II) in tetragonally compressed fashion by two μ_3–OH bridges (Figure 7b). Compared to 'paddlewheel' structures in case of copper(II)acetates[13] we take the advantage of perfluorinated carboxylate salt of copper(II) in the synthesis, which tend to form monomeric complexes.[31] Within the aggregate three different types of trifluroacetato groups were found (Figure 7a). These were $\mu_{1,3}$ bridging attached to Cu_2(μ-H_4L1) fragments, bidentate chelating for the central Cu3 atom and anionic, outside the coordination sphere. For bridging trifluroacetate the Cu−O−C−O/O−C−O−Cu torsion angle is 17.16/-5.28. The Cu_5 core of **3** is formed from trapping of central copper(II) center by two Cu_2(μ-H_4L1) fragments taking a shape of a modified hourglass (Figure 7d). The central copper(II) center chelated by trifluoacetate anions remains 3.194 and 3.345 Å apart from Cu^{II} centers within Cu_2(μ-H_4L1) fragments. The ligand bound and phenoxido-hydroxido bridged Cu···Cu separation is shortened to 2.909 Å.

View Article Online
DOI: 10.1039/C8NJ02131G

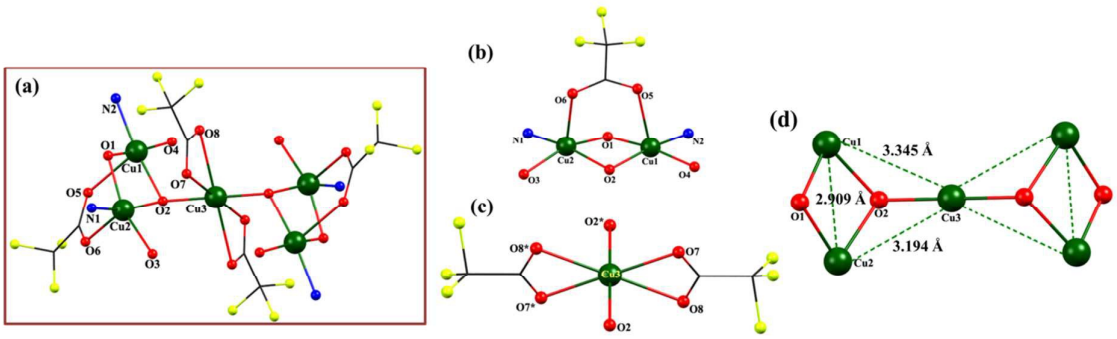

Figure 7.(a) Core view of the [Cu_5] unit; (b and c) coordination environments of Cu_2(μ-H_4L1) fragment and central Cu^{II}centre; (d) phenoxido and hydroxido bridges with **3**

Here also, the hydrogen-bonding interactions between the dangling alcohol arms of the ligand and trifluroacetate anions play the main role in the crystal packing with entrapment of trifluroacetate anions. Strong hydrogen-bonding interactions are seen between chelated imine alcohol arms bearing bound OH functions of the ligand with dangling alcohol arm (O3–H3A···O10) and with anionic trifluroacetate (O4–H4···O12). Also dangling free alcohol arm showed engagement with each other (O10–H10···O9) and with trifluroacetate (O9–H9···O12).[32] Involvement of μ_3–OH group is observed with trifluroacetate (O2–H2···O11) for a hydrogen bonded 2D sheet structure (Figure 8).

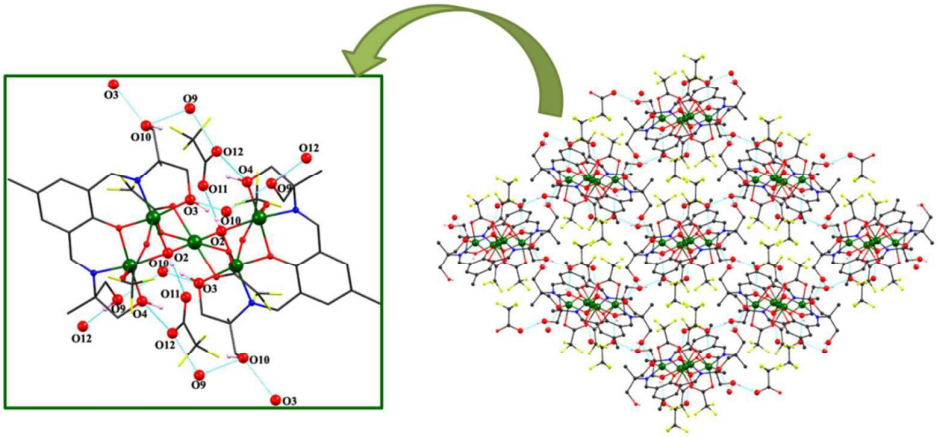

Figure 8 Intermolecular hydrogen bonding network resulted a 2D structure; inset: enlarged view of hydrogen bonding interactions involving trifluroacetates.

Structural Comparison of 1 with 2 and 3

In all three compounds each Cu^{II} center is bound by single imine N atom of ligand except Cu3 in **3**. The average Cu–N bond lengths in all the compounds are in 1.913 to 1.939 Å range. All together a variety of Cu–O bonds were found which differ from each with respect

View Article Online
DOI: 10.1039/C8NJ02131G

to the geometry and environment, *e.g.*, square pyramidal O_4N, and octahedral O_5N and O_6. Nine different Cu–O bonds are found from coordination of water, alcohol hydroxyl, bridging nitrate and perchlorate, bridging and chelated trifluoroacetate, bridging phenoxido and hydroxido groups. The longest ones in this set are from bridging perchlorato O atoms and next to these are from bridging nitrato O atoms. Water coordinated to the copper(II) center makes a large (2.549 Å) Cu–O separation in complex **1** compared to those in complex **2** (2.357 and 2.354 Å). The Cu–O bonds from bridging trifluoroacetate groups are longer than the chelated ones. The Cu–O bonds from bridging phenoxido group within $Cu_2(\mu\text{-}H_4L1)$ part in all the compounds are in 1.910–1.939 Å range. In **1** two types of coordination from nitrato anions stabilize the $Cu_2(\mu\text{-}H_4L1)$ in a particular manner different from a single perchlorato anion for clipping two $Cu_2(\mu\text{-}H_4L1)$ units in **2**. The μ_3–OH connection in **3**, connecting three Cu^{II} centers, provide one short (1.919 Å) and two long (1.975 and 1.995 Å) Cu–O bonds. Interestingly the coordination of Cu^{II} center to alcoholic OH arms has no effect with regard to C–O separation compared to the free and dangling arms. The trifluoroacetato-bridge clips the two Cu^{II} centers in **3** and also in bidentate chelating mode to the central Cu^{II} ion. In both the two cases the Cu–O separations are different, 2.201 and 2.301 Å in case of bridging mode and 1.976 and 2.048 Å for chelating mode. These two different modes of binding are responsible for varying the C–O bond distances in **3**. For bridging trifluoroacetate groups the C–O distances are 1.236 and 1.246 Å, whereas for chelating mode the same are 1.138 and 1.137 Å. The Cu−O−Cu angles within the $\{Cu_2(\mu\text{-}H_4L1)(OH)\}$ fragments is in 97.73−99.59° range for phenoxido bridges *vs.* 94.24−97.08° for hydroxido bridges. In **3**, the Cu−O(H)−Cu angle is further shortened due to the involvement of the μ_3−OH connector required for the growth of $[Cu_5]$ aggregate. In all the complexes, due to involvement in hydrogen bonding interactions, the H atom of the bridging hydroxide group remains out of plane with respect to the Cu_2O_2 diamond core. The geometrical features with respect the Cu−O(Ph)−Cu angle (α) (97.95 for **1**, 99.59 and 99.33 for **2**, and 97.74 for **3**), out-of-plane angle deviation (φ) (12.83 for **1**, 4.77 and 5.20 for **2** and 5.57 for **3**) and Cu−O−Cu−O torsion angle (τ) for the positioning of phenyl ring of bridging phenoxido group with respect to the molecular plane bearing the two Cu^{II} ions can modify the nature of magnetic interactions in the solid state (*vide supra*) (see Figure S4 in ESI).[33]

Mass Spectroscopic Evidence of Fragments

High Resolution ESI-MS Analysis. The existence of $Cu_2(\mu\text{-}H_4L1)$ based fragments in solution were established from mass spectral (ESI-MS positive) analysis of compounds **1**–**3**

View Article Online
DOI: 10.1039/C8NJ02131G

in MeOH solutions (Figures S5-S7 in ESI). Anion dependent charge neutralization of $Cu_2(\mu$-$H_4L1)$ unit formed in solution resulted in the $[Cu_2]$, $[Cu_4]$ and $[Cu_5]$ aggregates as compounds **1**–**3**. The analysis establishes the populations of key fragments in solution. All three compounds exhibited a common base peak at *m*/*z* = 240.02 which can be attributed to $[Cu_2(\mu–H_4L1)(\mu–OH)]^{2+}$ ($C_{17}H_{26}Cu_2N_2O_6$; Calcd 240.02) fragment in the solution phase. For **1**, the nitrato-bridged structure found in the solid state is not survived in MeOH solution medium and no other peaks of even smaller *m*/*z* value corresponding to any rational fragment is found in this analysis. The mass spectrum of **2** in MeOH medium records two peaks at *m*/*z* = 562.97 and 580.98 corresponding to the fragments $[Cu_2(\mu–H_4L1)(ClO_4)]H^+$ ($C_{17}H_{26}ClCu_2N_2O_9$; Calcd 562.99) and $[Cu_2(\mu–H_4L1)(\mu–OH)(ClO_4)]^+$ ($C_{17}H_{26}ClCu_2N_2O_{10}$; Calcd 580.98). Compared to the base peak of *m*/*z* = 240.02 for $[Cu_2(\mu–H_4L1)(\mu–OH)]^{2+}$ the relative intensity of these two peaks are less than 10% indicating poor abundance in solution. This is due to the fact that monodentate coordination of perchlorato anion is less stable than the bridging version as identified in **2** in the solid state (*vide supra*). In these two cases the monocationic charge states correspond to the species where one perchlorato anion is associated with the complex fragments. In case of complex **3** the mass spectrum displays a peak at *m*/*z* =575.01 corresponding to $[Cu_2(\mu–H_2L1)(CF_3COO)]H^+$ ($C_{19}H_{24}Cu_2F_3N_2O_7$; Calcd 575.01). The abundance of this species was found to be close to 40% of the base peak implying the presence of this species in considerable amount in solution compared to those obtained for compound **2**. Clearly this may be attributed to better coordinating potential of CF_3COO^- as compared to both NO_3^- and ClO_4^-. A low intensity peak at *m*/*z* = 596.99 corresponding to $[Cu_2(\mu–H_2L1)(CF_3COO)]Na^+$ ($C_{19}H_{23}Cu_2F_3N_2NaO_7$; Calcd 596.99) was also present in the spectrum of **3**.

MALDI-TOF Analysis. We have used this technique to create ions from all three compounds with nominal fragmentation. In search of higher nuclearity fragments in solution which might not have survived in the ESI process the compounds were subjected to MALDI-TOF analysis using 2,5-dihydroxybenzoic acid (DHBH) as the matrix. The spectrum of all the complexes exhibit a base peak at *m*/*z* = 339.61 corresponding to the protonated ligand $[H_5L1]H^+$ ($C_{17}H_{27}N_2O_5$; Calcd 339.19) along with a peak at *m*/*z* = 616.65 arising from $[Cu_2(\mu–H_4L1)(DHB)]^+$ ($C_{24}H_{30}Cu_2N_2O_9$; Calcd 616.05) (Figures S9–S11 in ESI). This later species is formed from the bridging coordination of carboxy end of the anionic matrix with dinuclear fragments observed in ESI-MS analysis ($[Cu_2(\mu–H_4L1)(\mu–OH)]^{2+}$). For **2** a peak at *m*/*z* = 371.42 is observed due to the presence of $[Cu_4(\mu–H_4L1)_2(\mu–OH)_2(\mu_{1,3}–ClO_4)(OH_2)_3]^{3+}$ ($C_{34}H_{58}ClCu_4N_4O_{19}$; Calcd 371.68) species in solution. The spectrum of **3** shows peaks at *m*/*z*

View Article Online
DOI: 10.1039/C8NJ02131G

= 678.61, 802.96, 864.94 and 1387.36 corresponding to the species $[Cu_2(\mu–H_4L1)(\mu–OH)(CF_3COO)(CH_3OH)_2]Na^+$ ($C_{21}H_{33}Cu_2F_3N_2NaO_{10}$; Calcd 679.05), $[Cu_3(\mu–H_4L1)(\mu–OH)(CF_3COO)_2(CH_3OH)]^+$ ($C_{22}H_{30}Cu_3F_6N_2O_{11}$; Calcd 802.96), $[Cu_3(\mu–H_4L1)(\mu–OH)(CF_3COO)_2(CH_3OH)_3]^+$ ($C_{24}H_{38}Cu_3F_6N_2O_{13}$; Calcd 865.01) and $[Cu_5(\mu–H_4L1)_2(\mu–OH)_2(CF_3COO)_2(CH_3OH)_3(H_2O)]Na^+$ ($C_{41}H_{67}Cu_5F_6N_4NaO_{20}$; Calcd 1387.06). This study thus clearly indicates the power of relatively soft technique responsible for low fragmentation while obtaining ions of aggregate compounds **2** and **3**. Thus in the gas phase it is possible to detect the formation of tetranuclear $[Cu_4(\mu–H_4L1)_2(\mu–OH)_2(\mu_{1,3}–ClO_4)]^{3+}$ and pentanuclear $[Cu_5(\mu–H_4L1)_2(\mu–OH)_2(CF_3COO)_2(CH_3OH)_3(H_2O)]Na^+$ species which ultimately crystallize in the solid state.

Reasoning behind the Isolated Products

The tuning of reaction conditions under which the $[Cu_2]$, $[Cu_4]$ and $[Cu_5]$ family formed, were analyzed in terms of anion dependence and synthetic environments. Competitive coordination of auxiliary anions to the metal ion centers influences the coordination aggregation process. Multinuclear bridging ability to connect more than two metal ions by NO_3^- ions is not frequently documented in the literature. Herein use of nitrate salt in the reaction medium trapped the product as $[Cu_2L]$ (**1**). Isolation of this dinuclear precursor from the reaction medium thus tempted us to examine the role of other anions for spontaneous self-aggregation reaction. Formation of $[Cu_4]$ species as complex **2** is dependent on the nature of the anion and the presence of perchlorate anion being a factor in its isolation as X-ray quality crystals. The highest possible bridging capacity of twelve metal ions by single ClO_4^- anion is known in $[Cu_{12}La_6]$ complex.[34] Connection of two Cu_2L fragments by a single ClO_4^- anion to provide the $[Cu_4]$ complex is not common in the literature.[35] The $\mu_{1,3}$ mode of one non-planar perchlorate anion functioning as bridging ligand led to the isolation of **2** while other three perchlorate anions were required for charge neutralization only. In case of **3** the reaction with $Cu(CF_3CO_2)_2{\cdot}4H_2O$ on the other hand resulted in the trapping of trifluoroacetate chelated copper(II) within the resulting $[Cu_5]$ complex. The trapping of $[Cu(CF_3CO_2)_2]$ unit by two $[Cu_2(H_4L1)(CF_3CO_2)]$ units, through μ_3–OH bridging, is responsible for the generation of new $[Cu_5]$ structural motif in Cu^{II}-carboxylate chemistry.

Electrochemistry

Further characterization in solution was achieved from cyclic voltammetric measurements in MeOH for **1-3.** The characteristic voltammetric responses for $\{Cu_2(\mu\text{-}H_4L1)\}$ fragments

View Article Online
DOI: 10.1039/C8NJ02131G

coming from all the compounds indicate their stability and aggregation behavior. A three-electrode setup was used consisting of a Pt working electrode, an Ag/AgCl reference electrode and a platinum auxiliary electrode.

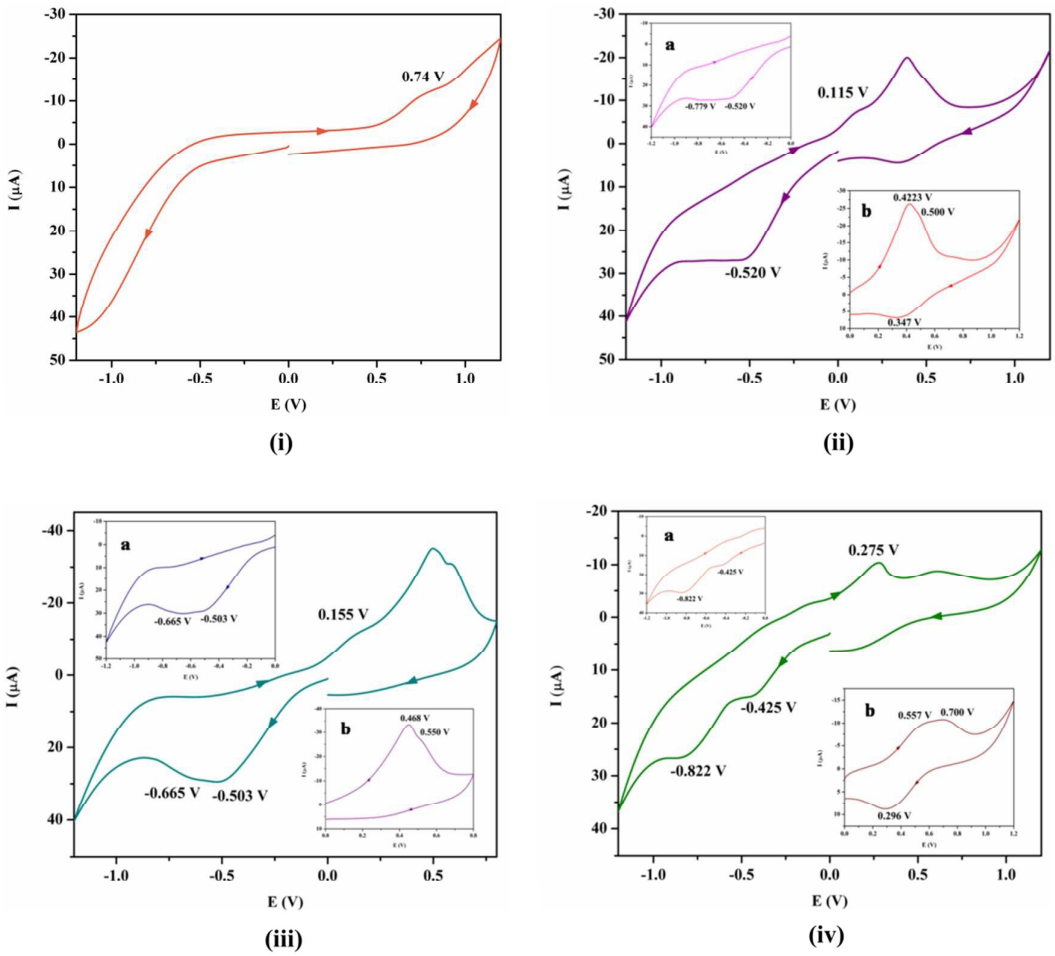

Figure 9 Cyclic voltammograms for (i) H_5L1, (ii) **1** [inset (a) from 0.0 V to -1.2 V, (b) from 0.0 V to 1.2 V], (iii) **2** [inset (a) from 0.0 V to -1.2 V, (b) from 0.0 V to 0.8 V] and (iv) **3** [inset (a) from 0.0 V to -1.2 V, (b) from 0.0 V to 1.2 V] in MeOH containing 0.1 M nBu_4NClO_4 as supporting electrolyte at 298 K, at platinum working electrode, at a scan rate of 100 mV s^{-1}, using Ag/AgCl as the reference electrode

For H_5L1 in MeOH an irreversible anodic peak at 0.74 V at a sweep rate of 0.1 V s^{-1} was obtained for ligand centered oxidation (Figure 9-i). For **1** two closely spaced irreversible reductions were recorded at E_{pc} = −0.520 and −0.779 V respectively, for the electron transfer processes $Cu^{II}Cu^{II} \rightarrow Cu^{I}Cu^{I}$ and $Cu^{I}Cu^{I} \rightarrow Cu^{0}Cu^{0}$ within $\{Cu_2(\mu\text{-}H_4L1)\}$ fragment. During the reverse scan a small peak at 0.115 V is found due to anodic stripping, which is absent when scanned between 0.0 V and 1.2 V. The irreversible oxidative response at E_{pa} = 0.422 V is most probably due to $Cu^{II}Cu^{II} \rightarrow Cu^{III}Cu^{III}$ oxidation (Figure 9-ii-b inset). On scan reversal

View Article Online
DOI: 10.1039/C8NJ02131G

from 1.2 V, a small cathodic peak at E_{pc} = 0.347 V is seen for the reduction of unstable $Cu^{III}Cu^{III}$ fragment to $Cu^{II}Cu^{II}$ species ($i_{pc}/i_{pa}\neq1$). The response for **2** is similar to that found for **1** with irreversible cathodic reductions at E_{pc} = −0.503 V and−0.665 V respectively with anodic stripping at 0.155 V. The irreversible oxidative response for $Cu^{II}Cu^{II} \rightarrow Cu^{III}Cu^{III}$ occurs at E_{pa} = 0.468 V (Figure 9-iii-b inset).

The nature of voltammogram for **3** is different from both **1** and **2**. Now two well separated irreversible reductive responses were observed at E_{pc} = −0.425 V and −0.822 V corresponding to $Cu^{II}Cu^{II} \rightarrow Cu^{I}Cu^{I}$ and $Cu^{I}Cu^{I} \rightarrow Cu^{0}Cu^{0}$. Herein the anodic stripping potential for Cu^0 from the electrode surface was found at 0.275 V. Scanning in the positive direction resulted two irreversible oxidations at E_{pa}= 0.557 V and E_{pa} = 0.700 V, of which the latter was due to ligand centered oxidation (E_{pa} for H_5L1 = 0.730 V). The former response is due to $Cu^{II}Cu^{II} \rightarrow Cu^{III}Cu^{III}$ oxidation and the corresponding reduction of $Cu^{III}Cu^{III} \rightarrow Cu^{II}Cu^{II}$ is found at E_{pc} = 0.296 V. The ΔE_p value found to be 261 mV ($E_{1/2}$ = 0.426 V) and i_{pc}/i_{pa} ratio ≈ 1 indicate some stability of $Cu^{III}Cu^{III}$ species within cyclic voltammetric time scale. The similar nature of the voltammograms for **1** and **2** suggest the existence of $[Cu_2(\mu–H_4L1)(\mu–OH)]^{2+}$ fragments in MeOH solutions in both the two cases as also evidenced from the ESI-MS analysis *(vide supra)*. For **3** the distinct responses were found from species like $[Cu_2(\mu–H_2L1)(CF_3COO)]H^+$ having 40% abundance to that of the base peak in ESI-MS analysis.

EPR Spectra

X-band EPR spectra for powdered samples of **2** and **3** were measured at 298 K and 75 K (Figure 10). An axial EPR signal was observed for **2** with $g_{\|}$ = 2.264 and $g_{\perp}$= 2.04 (g_{av} = 2.114) (Figure 10-i). The average nuclear hyperfine constants are, $A_{\|}$ = 180.6 G and $A_{\perp}$ = 41.66 G and no resonances below 1050 G and above 3850 G were detected. For **3** a different type of axial spectrum was obtained (Figure 10-ii). At 75 K hyperfine features of the parallel component were observed with a small $A_{\|}$ value of 65.79 G. The g-tensors were found to be $g_{\|}$ = 2.28 and $g_{\perp}$= 2.10. The weak intensity, forbidden half field (ΔM_S = ±2) signals were observed at 1605 G (g = 4.298) and 1605.5 G (g = 4.296) for **2** and **3** respectively, clearly indicating the presence of spin-spin interactions. Unfortunately **1** gave poor quality spectra from which reliable A and g values could not be determined.

View Article Online
DOI: 10.1039/C8NJ02131G

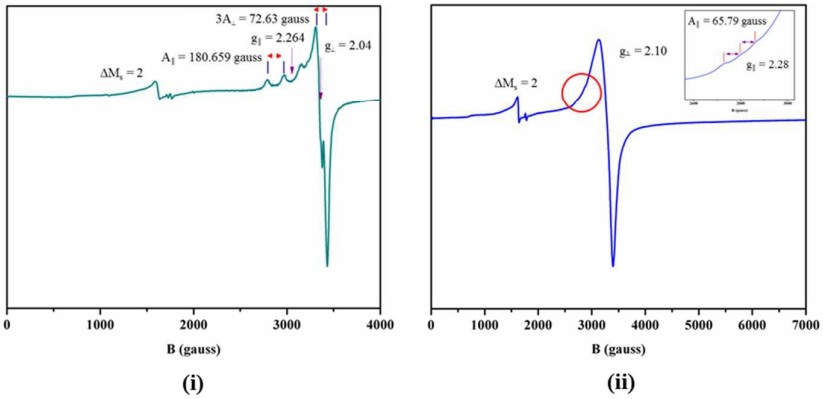

Figure 10 X-band EPR spectra at 298 K and 75 K for microcrystalline samples of **2** (i) and **3** (ii) respectively

The X-band EPR spectrum for a polycrystalline sample of **3** in the temperature range 5 K – 115 K is shown in Figure 11 (i). At 5 K one broad symmetric transition was observed at 3312 G without any hyperfine feature. The intensity of the signal is temperature dependent and showed maxima at 10 K. Further rise in temperature led to continuous decrease in signal intensity. The rate of decrease of signal intensity is high upto 35 K then gradually decreasing at higher temperatures. The g value at the same time increases from 2.09 at 5 K to 2.12 at 115 K. This sort of change in signal intensity with rise in temperature is consistent with the presence of antiferromagnetic coupling interactions within the copper centers. The spectrum at 10 K shows the highest intensity band centered at g = 2.09 (3318 G for ν = 9.7196 GHz). Simulation of the spectrum[36,37] considering a system with three electrons and three copper nuclei lead to a reasonable fit yielding the following gyromagnetic factors: $g_1 \approx g_2 = 2.04$ ($g_\perp$) and $g_3 = 2.20$ ($g_\parallel$) (Figure 11(ii)). The g_{av} value of 2.09 obtained from the simulated data is in good agreement with that found experimentally. The g-values of axial spectrum are related by the expression[38] $G = (g_\parallel\text{-}2.003)/(g_\perp\text{-}2.003)$ and is a measure for exchange interactions between the Cu^{II} centers as measured in the solid state. When G < 4.0, there is substantial exchange interaction in the polycrystalline sample.[38,39] In our case the G value for **3** is 5.324 demonstrating the presence of weak interactions which is in agreement with the magnetic and DFT studies. The absence of fine structures at the low temperatures (< 75 K) is consistent with the presence of intercluster exchange interactions that tend to average out the fine structures arising from the multiplets.[40] The hyperfine features in the parallel component is observed at 75 K which is not distinguishable at room temperature due to signal broadening. The $A_\parallel$ value of 65.79 G is 2.7 times smaller than that obtained for isolated Cu^{II} site and in case of complex **2** ($A_\parallel \approx 180$ G).

View Article Online
DOI: 10.1039/C8NJ02131G

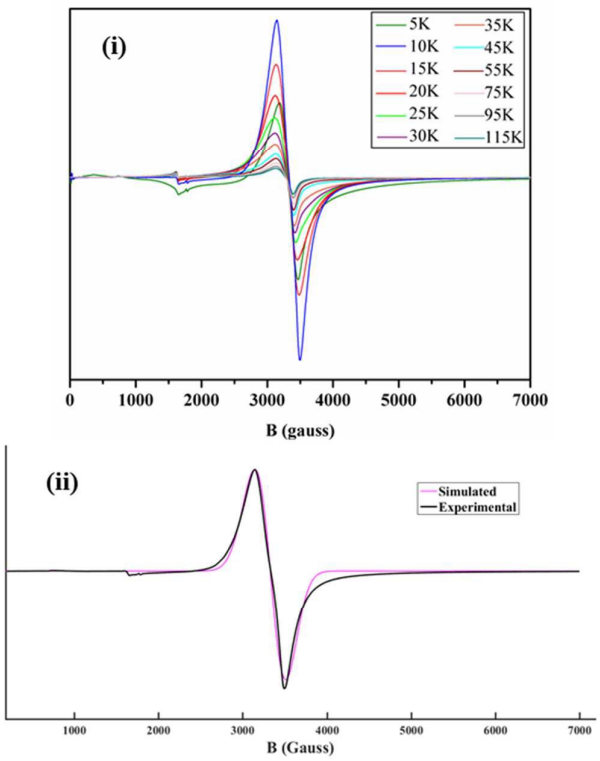

Figure 11 (i) X-band EPR spectra at 5 K to 115 K for microcrystalline sample of **3**. (ii) Overlapping experimental and simulated EPR spectra of **3** at 10 K

Magnetic Measurements

The temperature dependence of the molar magnetic susceptibility, χ_M, of **1**–**3** was measured under a magnetic field of 1 T for **1** and 0.1 T for **2** and **3** over the temperature range 290 – 2 K. Plots of $\chi_M T$ versus temperature, T, for compounds **1** and **3** is shown in Figure 12. At 290 K, the values of $\chi_M T$ are 0.78 (**1**) and 1.96 $cm^3\ mol^{-1}\ K$ (**3**), which is consistent with the expected values for two Cu^{II} sites in case of **1** (0.75 $cm^3\ mol^{-1}$ K, for $g = 2.0$) and five Cu^{II} centers for **3** (1.875 $cm^3\ mol^{-1}$ K, for $g = 2.0$). For both the compounds, a decrease in $\chi_M T$ is observed upon lowering the temperature, with the data entering a plateau at low temperatures. For **1**, the value of $\chi_M T$ is very close to zero below 20 K, reaching a minimum value of 0.002 $cm^3\ mol^{-1}$ K measured at 2 K. In the case of **3**, the $\chi_M T$ data also enter a plateau below 20 K, where $\chi_M T = 0.51\ cm^3\ mol^{-1}$ K, with a further slight decrease to $\chi_M T = 0.44\ cm^3\ mol^{-1}$ K at 2 K. These data indicate overall antiferromagnetic exchange interactions in both compounds. To determine the size of the exchange, the data were fitted using the program Phi 2.0.[41] The data for **1** were fitted considering one coupling constant arising from the interaction between the two Cu^{II} ions, J_1 (Figure S15, ESI), and also by allowing the g-value to vary freely. A

View Article Online
DOI: 10.1039/C8NJ02131G

small paramagnetic impurity of 1% (S = ½) was also included in the fit. The Hamiltonian used for the fitting procedure was:

$$\hat{H} = -2J_1(\hat{S}_{Cu1}\hat{S}_{Cu2}) + g\mu_B H\sum_{i=1}^{2}\hat{S}_i$$

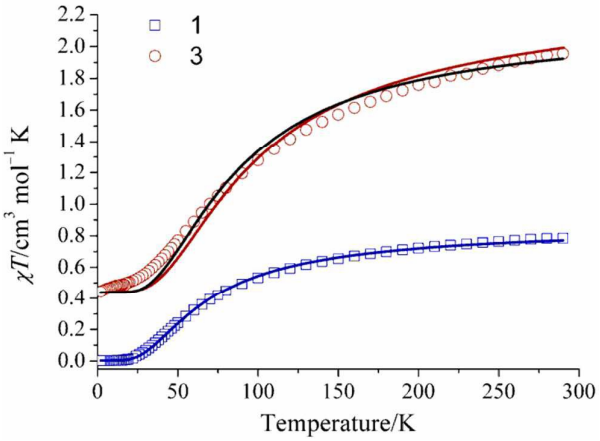

Figure 12 $\chi_M T$ versus T plot for **1** and **3**. The solid blue line represents a fit of the data for **1**, while the solid black line is the fit of the data for **3** and the red line is a simulation based on the results of DFT calculations (see text for details)

and the resulting curve is shown in Figure 12. The strength of the exchange interaction J_1 was found to be −42.9 cm^{-1}, and the g-value yielded was 2.16. It is difficult to offer a direct comparison of these values with other compounds in the literature, as there are very few examples of two hexa-coordinate Cu^{II} centers bridged by one phenoxido, one hydroxido, and one nitrato group. For dinuclear Cu^{II} complexes containing two hydroxido bridges, a linear correlation was found between the coupling constant J and the size of the Cu−O−Cu angle, with larger angles leading to stronger antiferromagnetic exchange.[42] However, this exchange interaction was also found to be dependent on the extent of displacement of the hydrogen atom of the hydroxido bridges away from the Cu_2O_2 plane, with large displacements leading to much weaker antiferromagnetic exchange or even ferromagnetic exchange interactions.[43,44] We therefore used B3LYP/6-31+G* calculations (broken symmetry approach, see theoretical methods) to evaluate the magnetic coupling constant J in **1**. The theoretical value of J (−36.9 cm^{-1}) is in good agreement with the experimental one (−42.9 cm^{-1}) and confirms the anti-ferromagnetic coupling. To investigate the mechanism for the magnetic exchange coupling, the spin density distribution was analyzed. The atomic spin population values on the Cu^{II} centers and the donor atoms of the ligands are listed in Table 1.

View Article Online
DOI: 10.1039/C8NJ02131G

Table 1 Atomic spin densities (e) computed for the high and low spin configuration of **1** at the B3LYP/6-31+G*

Atom Label	High spin	Low Spin
Cu1	0.71	0.73
Cu2	0.67	-0.68
N1	0.11	0.11
N2	0.10	-0.10
O1	0.15	-0.03
O2	0.22	-0.02
O3	0.02	0.02
O4	0.03	-0.03

For the high-spin (HS) configuration, the Mulliken spin population data shows that some spin (*ca.* 0.62 e) is delocalized through the ligands, and the rest (1.38 e) is supported by the Cu^{II} centers. The spin density plots corresponding to one of the 'broken-symmetry' wave function and the high-spin state for **1** are described in Figure 13, where α and β spin states are denoted by positive (blue) and negative (green) signs, respectively. The broken-symmetry spin population values at the magnetic centers are +0.73 on Cu(1) and −0.68 on Cu(2) and the spin delocalization is considerable (~30% of the spin is delocalized to the ligand framework). The spin on the phenoxide and hydroxide O atoms (O1/O2) is ca. 0.37 e in the HS state and −0.05 e in the broken-symmetry state of **1**, consequently, the bridging oxygen atoms mediate the magnetic exchange. Plots of the magnetic orbitals are given in the ESI (Figure S13) showing the contribution of $d_{x^2-y^2}$ atomic orbitals of the Cu^{II} centers along with the p_x and p_y orbitals of the bridging O atoms.

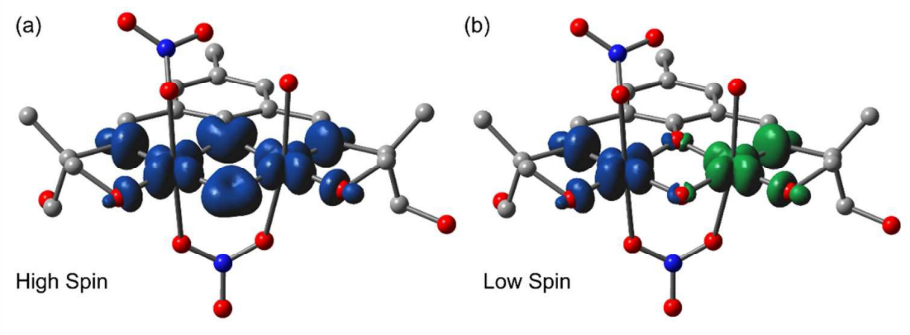

Figure 13 Representation of spin density (contour 0.004 e $Å^{-3}$) at the high spin (a) and low spin (b) configurations of **1**. Positive spin represented in blue and negative spin in green

View Article Online
DOI: 10.1039/C8NJ02131G

For **3**, the fits were initially attempted using a model involving three distinct exchange interactions considering the topology of the complex as a pair of scalene triangles sharing a vertex (Cu3). However, this led to physically unreasonable exchange interactions, with the interaction between Cu1 and Cu3 or Cu2 and Cu3 found to be as strong as the interaction between Cu1 and Cu2, despite the significant differences in distance between the pairs of atoms and in their connectivity. Therefore, the data were fitted considering one exchange interaction J_1 between Cu1 and Cu2, (Figure S15 in ESI) and their symmetry equivalent counterparts, adopting an approach used previously for a compound containing a related ligand and the same topology.[29] The *g* values for the five Cu(II) ions were fixed at 2.16 based on the results for the fitting procedure for compound **1**. The Hamiltonian was therefore:

$$\hat{H} = -2J_1\left(\hat{S}_{Cu1}\hat{S}_{Cu2} + \hat{S}_{Cu1^*}\hat{S}_{Cu2^*}\right) + g\mu_B H\sum_{i=1}^{5}\hat{S}_i$$

yielding a value for $J_1 = -54.2$ cm^{-1} (shown as the black curve in Figure 12). Simulations including weaker interactions between Cu1 and Cu2 and the central Cu3 ion did not lead to better agreement with the experimental data. DFT calculations indicated an antiferromagnetic interaction between Cu1 and Cu2 of −61 cm^{-1}, and ferromagnetic exchange between the Cu3 center and Cu1 and Cu2 centers of +2.5 cm^{-1}. The most notable aspect of all of the exchange interactions described is that they are relatively weak for coupling between the Cu^{II} centers, and that they are significantly weaker than the interactions mediated by other related ligands.[29,10]

As aforementioned, the B3LYP/6-31+G* calculation of the Cu1–Cu2 interaction in compound **3** reveals an antiferromagnetic coupling with $J = -61.1$ cm^{-1}, that is in good agreement with the experimental one (−54.2 cm^{-1}). To investigate mechanism for the magnetic exchange coupling, the spin density distribution was studied. The atomic spin population values on the Cu1 and Cu2 metal centers and the O1 and O2 bridging donor atoms of the ligands are listed in Table 2.

Table 2 Atomic spin densities (e) computed for the High and Low spin configuration of compound **3** at the B3LYP/6-31+G*

Atom Label	High spin	Low Spin
Cu1	0.68	–0.68
Cu2	0.69	0.71
N1	0.13	-0.14

View Article Online
DOI: 10.1039/C8NJ02131G

N2	0.14	0.14
O1	0.16	0.01
O2	0.12	0.00
O3	0.03	-0.03
O4	0.03	0.03

For the high-spin (HS) configuration, the Mulliken spin population data shows that a noticeable spin (ca. 0.63 e) is delocalized through the ligands, and the rest (1.37 e) is supported by the Cu magnetic centers (see Table 2). The spin density plots of the "broken-symmetry" wave function and the high-spin state for complex **3** are described in Figure 14, where α and β spin states are represented by blue and negative (green) signs, respectively. The broken-symmetry spin population values at the magnetic centers are +0.71 on Cu(1) and −0.68 on Cu(2) and the spin delocalization is considerable (~30% of the spin is delocalized to the ligand framework). The spin on the phenoxide and hydroxide O atoms (O1/O2) are 0.16 and 0.12 e in the HS state and negligible in the broken-symmetry state of complex **3**, thus confirming that the bridging oxygen atoms mediate the magnetic exchange.

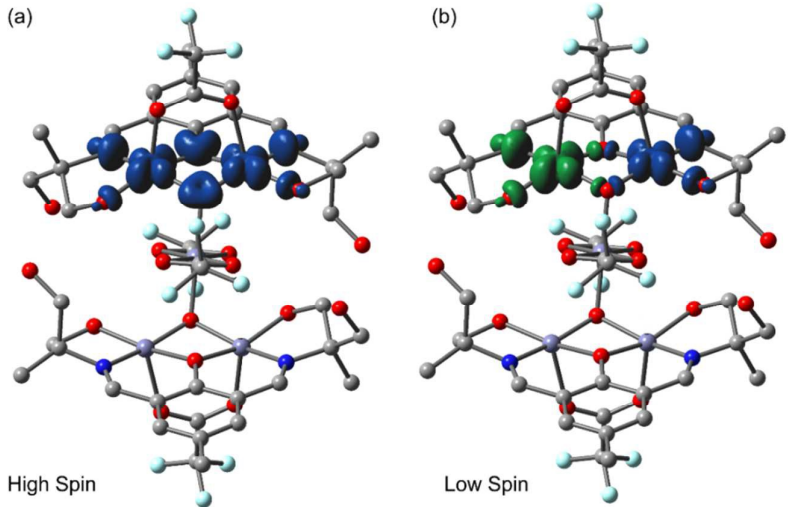

Figure 14 Representation of spin density (contour 0.004 e $Å^{-3}$) at the high spin (a) and low spin (b) configurations of complex **3**. Positive spin represented in blue and negative spin in green

Finally, we have also studied the magnetic behavior of compound **2** using DFT calculations. We have initially analyzed three distinct exchange interactions (Cu1-Cu2, Cu3-Cu4 and Cu2-Cu4). The magnetic interaction between Cu2 and Cu4 ($\mu_{1,3}$–ClO_4 bridging, Cu···Cu separation > 7Å) was found to be inexistent (J = 0). In contrast, the B3LYP/6-31+G* calculation of Js between Cu1 and Cu2 and between Cu3 and Cu4 showed the existence of antiferromagnetic coupling (–99.1 cm^{-1} and –90.0 cm^{-1}, respectively). Thus the J values

View Article Online
DOI: 10.1039/C8NJ02131G

predicted for this compound are slightly larger in absolute value than those observed for compounds **1** or **3**. The atomic spin densities and spin density plots for compound **2** are given in the ESI (see Figure S14 and Tables S3 and S4). Unfortunately we were unable to obtain good magnetic data for **2**, due to the presence of a paramagnetic impurity that dominated the data in the low temperature region, where a well-isolated $S = 0$ ground state can be expected based on the DFT calculations. The magnetic data for compound **2** together with a simulation based upon the results of the DFT calculations are shown in Figure S16 in ESI.

Experimental Section

Reagents and Materials

The chemicals used were obtained from the following sources: trifluroacetic acid (99%) from SRL, India, copper(II) carbonate hydroxide, copper(II) nitrate trihydrate and triethylamine from Merck, India and 2-amino-2-methyl-1,3-propanediol from Alfa Aesar. Copper(II) perchlorate hexahydrate was freshly prepared by treating hydrated copper(II) carbonate (22.12 g, 0.1 mol) with 1:1 aqueous solution of perchloric acid. Similarly copper(II) trifluroacetate was obtained by reacting copper(II) carbonate (11.06 g, 0.05 mol) with trifluroacetic acid (11.40 g, 0.1 mol) in water. 2,6-diformyl-4-methylphenol was prepared following a modified literature procedure providing better yield.[45] All the chemicals and solvents used in this work were reagent-grade materials and were used as received without further purification.

Synthesis

Ligand H_5L1 [2,6-bis-{(1,3-dihydroxy-2-methylpropan-2-ylimino)methyl)}-4-methylphenol]. The Schiff base ligand H_5L1 was prepared by reacting 4-methyl-2,6-diformylphenol (0.820 g, 5 mmol) and 2-amino-2-methyl-1,3-propanediol (1.05 g, 10 mmol) under stirring condition for 1 h followed by refluxing for another 2 h. The solvent was removed under vacuum to yield a yellow oily mass, which was characterized by FTIR, NMR spectroscopy and used directly without further purification. FT-IR (cm^{-1}, KBr pellet): 3341 (br), 1638 (m), 1219 (w), 1052 (w), 772 (vs). ^1H NMR (600 MHz, $(CD_3)_2SO$, δ ppm): 8.61 (2H, imine–H), 7.55 (2H, aromatic–H), 3.42 (8H, $–OCH_2$), 2.50 (3H, $–CH_3$ substituent on phenyl ring), 1.18 (6H, $–CH_3$). ^{13}C NMR (150 MHz, $(CD_3)_2SO$, δ ppm): 163.58 (imine C), 124.78–160.01 (aromatic C), 66.06 (methylene C attached with O), 63.72 (tertiary C attached to imine N), 22.65 (methyl C attached with benzene ring), 18.63 (methyl C).

View Article Online
DOI: 10.1039/C8NJ02131G

$[Cu_2(\mu\text{–}H_4L1)(\mu\text{–}OH)(\mu_{1,3}\text{–}NO_3)(NO_3)(OH_2)]\cdot H_2O$ (1). The as-prepared solution of H_5L1 (25 mL), containing 1 mmol of H_5L1 (*approx*. 0.33 g), was diluted to 30 mL by MeOH. To this, a MeOH solution (15 mL) of copper(II) nitrate trihydrate (0.485 g, 2 mmol) was added slowly and the resulting green solution was stirred for *ca.* 15 min. Following this, a MeOH solution (10 mL) of sodium acetate (0.164 g, 2 mmol) was added during which the solution color changed to dark green and the stirring was continued for 1 h. The solution was filtered, mixed with equal volume of MeCN and kept in air at room temperature for slow evaporation. Green block shaped single crystals suitable for X-ray analysis were obtained after 8 days from this MeOH-MeCN (1:1) solvent mixture. Yield: 0.35 g (54%). Anal.calc. for $C_{17}H_{30}Cu_2N_4O_{14}$ (641.55 g mol^{-1}): C, 31.83; H, 4.71; N, 8.73. Found: C, 31.91; H, 4.74; N, 8.74. Selected FT-IR bands: (KBr, cm^{-1}, vs=very strong, br=broad, s=strong, m=medium, w=weak): 3400 (br), 1635 (vs), 1384(vs). UV-vis spectra [λ_{max}, nm (ε, L mol^{-1} cm^{-1})]: (MeOH solution) 645 (67), 368 (7600).

$[Cu_4(\mu\text{–}H_4L1)_2(\mu\text{–}OH)_2(\mu_{1,3}\text{–}ClO_4)(OH_2)_2](ClO_4)_3\cdot 2H_2O$ (2). Complex **2** was prepared following a similar procedure as described above for **1** using $Cu(ClO_4)_2\cdot 6H_2O$ (0.74 g, 2 mmol) instead of $Cu(NO_3)_2\cdot 3H_2O$. Green block shaped crystals suitable for X-ray analysis were obtained after 1 week. Yield: 0.494 g (69%). The elemental analysis data confirms the molecular formula $[Cu_4(\mu\text{–}H_4L1)_2(\mu\text{–}OH)_2(\mu_{1,3}\text{–}ClO_4)(OH_2)_2](ClO_4)_3\cdot 2H_2O$. Anal calc. for $C_{34}H_{60}Cl_4Cu_4N_4O_{32}$ (1432.85 g mol^{-1}): C, 28.50; H, 4.22; N, 3.91. Found: C, 28.08; H, 4.13; N, 3.80. Selected FT-IR bands: (KBr, cm^{-1}, vs=very strong, br=broad, s=strong, m=medium, w=weak): 3338 (br), 1636 (s), 1142 (vs), 1111 (vs), 1088 (vs). UV-vis spectra [λ_{max}, nm (ε, L mol^{-1} cm^{-1})]: (MeOH solution) 666 (129), 374 (10500).

$[Cu_5(\mu\text{–}H_4L1)_2(\mu_3\text{–}OH)_2(\mu_{1,3}\text{–}O_2CCF_3)_2(O_2CCF_3)_2](CF_3COO)_2$ (3). To a stirred 'solution of H_5L1' (*approx*. 0.33 g, 1 mmol) in MeOH (20 mL), a MeOH solution (10 mL) of $Cu(CF_3COO)_2\cdot 4H_2O$ (0.904 g, 2.5 mmol) was added. The resulting green solution was stirred for 2 h. Then the solution was filtered and kept for slow evaporation in air. Green block shaped single crystals suitable for X-ray analysis were obtained after 1 week from the MeOH reaction medium. Yield: 0.69 g (81%). Microanalytical data are consistent with the formula $[Cu_5(\mu\text{–}H_4L1)_2(\mu_3\text{–}OH)_2(\mu_{1,3}\text{–}O_2CCF_3)_2(O_2CCF_3)_2]\cdot(CF_3COO)_2$. Anal. calc. for $C_{46}H_{52}Cu_5F_{18}N_4O_{24}$ (1704.67g mol^{-1}) C, 32.41; H, 3.07; N, 3.29. Found: C, 32.47; H, 3.10; N, 3.31. Selected FT-IR bands: (KBr, cm^{-1}, vs=very strong, br=broad, s=strong, m=medium, w=weak) 3348 (br), 1670 (vs), 1644 (s) 1431 (m), 1329 (m). UV-vis spectra [λ_{max}, nm (ε, L mol^{-1} cm^{-1})]: (MeOH solution) 678 (104), 371 (13700).

View Article Online
DOI: 10.1039/C8NJ02131G

Caution! *Complexes of metal ions containing organic ligands along with perchlorate counter anions are explosive in nature. Though we have not faced any problem while dealing with the title compounds, but it is safe to prepare small amount of sample and handle it with care.*

Physical Measurements

Elemental analyses (C, H and N) of the compounds were performed with a PerkinElmer model 240C elemental analyzer. A Shimadzu UV 3100 UV–vis–NIR spectrophotometer and a PerkinElmer RX1 spectrometer were used to record the solution electronic absorption spectra and FTIR spectra respectively. The purity of the powder compounds was determined by powder X-ray diffraction (PXRD) patterns using a Bruker AXS X-ray diffractometer (40 kV, 20 mA) using Cu-K_α radiation (λ = 1.5418 Å) within 5–50° (2θ) angular range and a fixed-time counting of 4s at 25 °C. A Bruker esquire 3000 plus mass spectrometer was employed to collect the electrospray ionization (ESI) high resolution mass spectra of the three compounds. MALDI-TOF MS studies were performed with the DHBH (2,5-dihydroxybenzoic acid) matrix by using a Bruker UltrafleXtreme instrument. CHI 1120A electrochemical analyzer was used for cyclic voltammetric measurements. Electrochemical measurements were performed at 25°C in MeOH in one compartment cell with platinum as working electrode, Pt wire as counter electrode and Ag/AgCl as reference electrode. Electron paramagnetic resonance (EPR) spectra were recorded at 9.13 GHz (X-band) in continuous wave mode with a Bruker ELEXSYS 580 X-band EPR spectrometer equipped with a standard accessory for room temperature operation (298 K).

Magnetic Measurements

Direct current (dc) magnetic measurements were performed on polycrystalline samples of compounds **1** and **3** constrained in eicosane, using a Quantum Design SQUID magnetometer equipped with a 5 T magnet. The dc measurements were carried out in the temperature range 290 – 2.0 K under applied fields of 1 T (**1**) and 0.1 T (**2** and **3**). Data were corrected for the diamagnetism of the compounds and for the diamagnetic contributions of the sample holder and eicosane through measurements.

Crystal Data Collection and Refinement

Single crystal X-ray diffraction data for **1**- **3** were collected on a Bruker SMART APEX-II CCD X-ray diffractometer furnished with a graphite-monochromated Mo Kα (λ = 0.71073 Å) radiation by the ω scan (width of 0.3° frame^{-1}) method at 293 K with a scan rate of 4 s per frame. SAINT and XPREP software[46] were used for data processing and space group

View Article Online
DOI: 10.1039/C8NJ02131G

determination. Direct method of SHELXS-2014[47] were used to solve the structure and then refined with full-matrix least squares using the SHELXL (2014/7)[48] program package included into WINGX system Version *2014.1*.[49] Data were corrected for Lorentz and polarization effects; an empirical absorption correction was applied using the SADABS.[50] The locations of the heaviest atoms (Cu) were determined easily. The O, N, and C atoms were subsequently determined from the difference Fourier maps. These atoms are refined anisotropically. The H atoms on the bridging hydroxide were found in the difference Fourier maps and refined isotropically. The remaining H atoms were incorporated at calculated positions and refined with fixed geometry and riding thermal parameters with respect to their carrier atoms. Crystallographic diagrams were presented using DIAMOND software.[51] A summary of the crystal data and relevant refinement parameters is summarized in Table 3. Short distance of 0.96 Å between H14C and H16D is due to the disorder of C16. Crystallographic data have been deposited with the Cambridge Crystallographic Data Centre as supplementary publications CCDC-1828020, 1828021, 1828022. These data can also be obtained free of cost at www.ccdc.cam.ac.uk/conts/retrieving.html (or from the Cambridge Crystallographic Data Centre).

Table 3 Crystal data and structure refinement details for **1** to **3**

parameters	**1**	**2**	**3**
Formula	$C_{17}H_{30}Cu_2N_4O_{14}$	$C_{34}H_{60}Cl_4Cu_4N_4O_{32}$	$C_{46}H_{52}Cu_5F_{18}N_4O_{24}$
F.W. (g mol^{-1})	641.55	1432.85	1704.67
crystal system	Monoclinic	Triclinic	Monoclinic
space group	$P\,2_1/n$	$P\bar{1}$	$P\,2_1/c$
Crystal color	Green	Green	Green
Crystal size/mm^3	0.37×0.27×0.18	0.38×0.28×0.17	0.36×0.25×0.17
a/ Å	9.4758(14)	13.616(3)	14.1130(14)
b/ Å	8.9390(13)	14.129(3	17.8567(18)
c/ Å	28.633(4)	15.755(4)	12.4740(12)
α/ deg	90.00	105.525(6)	90.00
β/ deg	95.851(4)	94.758(6)	107.507(3)
γ / deg	90.00	112.669(6)	90.00
V/ Å^3	2412.7(6)	2635.1(11)	2998.0(5)
Z	4	2	2
D_c/g cm^{-3}	1.766	1.803	1.888
μ (mm^{-1})	1.842	1.896	1.884
F(000)	1320	1460	1710
T/K	293(2)	293(2)	293(2)

View Article Online
DOI: 10.1039/C8NJ02131G

Total reflns	27569	33413	38111
R(int)	0.1097	0.0345	0.0571
Unique reflns	4802	10379	6114
Observed reflns	3875	9010	4782
Parameters	368	743	455
R_1; wR_2 ($I > 2\sigma(I)$)	0.0875, 0.2050	0.0372, 0.1053	0.0576, 0.1679
GOF (F^2)	1.138	1.040	1.069
Largest diff peak and hole (e Å^{-3})	2.111, -2.075	1.084, -0.791	1.477, -0.935
CCDC No.	1828020	1828021	1828022

$R_1 = \Sigma(||F_o|-|F_c||)/\Sigma|F_o|$. $wR_2 = [\Sigma w(|F_o|-|F_c|)^2/\Sigma w(F_o)^2]^{1/2}$. $w = 0.75/(\sigma^2(F_o) +0.0010F_o^2)$

Theoretical Studies

The magnetic properties of compounds **1**, **2** and **3** were calculated using the Gaussian 09 package[52] by means of the density functional theory (DFT) and the broken symmetry approach.[53,54,55] We have used the hybrid B3LYP[56] functional combined with the 6-31+G* basis set,[57] which is a good compromise between the size of the systems and the accuracy of the method. We have utilized the crystallographic coordinates and optimized the positions of the hydrogens to carry out the calculations. Moreover, the theoretical models were simplified using H atoms instead of methyl groups in the ligand.

For the calculations of the pentanuclear complex **3**, we evaluated each individual coupling constant (J_1 and J_2) using the methodology proposed by Alvarez group[58,59] in mutinuclear systems. This methodology comprises the substitution of paramagnetic centers by diamagnetic ones to simplify the calculation of coupling constants to evaluations for magnetically coupled systems. This methodology is accurate and very convenient to estimate coupling constants individually.

Conclusions

We have demonstrated for the first time the use of same Schiff base H_5L1 for the synthesis of [Cu_2], [Cu_4] and [Cu_5] complexes. Involvement of NO_3^-, ClO_4^- and $F_3CCO_2^-$ groups has been systematically examined for their specificity and anion binding dependent aggregation. The study also recognized the potential of H_5L1 in phenoxido form to enforce the formation of the Cu^{II} aggregates of varying nuclearity and structure. From the imine side arms one of the protonated alcohol end showed coordination whereas the other adjacent one remained dangling to contribute for hydrogen bonding interactions and stabilization of the entities in crystals. Structures in three dimension and bridging potential of NO_3^-, ClO_4^- and $F_3CCO_2^-$

View Article Online
DOI: 10.1039/C8NJ02131G

between Cu^{II} centers are crucial in guiding the final outcome of different reactions. Charge density within the products was important to obtain neutral [Cu_2], and cationic [Cu_4] and [Cu_5] compounds. Both ESI-MS (positive) and MALDI-TOF studies indicated the presence of ligand bound {Cu_2(μ-H_4L1)} fragments in solution and thus allowed fine-tuning of aggregation in presence of NO_3^-, ClO_4^- and $F_3CCO_2^-$ ions during solid state separation and crystallization. Solution phase characterization was also done by cyclic voltammetry analysis. Only NO_3^- as ancillary ligand is appropriate for the isolation of **1**. Whereas ClO_4^- ion, as a very rare example, could bridge two {Cu_2(μ-H_4L1)} fragments in **2**. We have shown that {Cu_2(μ-H_4L1)(μ-OH)}$^{2+}$ units, resulting from H_4L1^- and water derived HO^- bridges, and characterized by HRMS analysis, were accountable for the trapping of {$Cu(O_2CCF_3)_2$} units to give **3**. The magnetic exchange interactions found for the complexes were weaker than those normally found for related Cu^{II} base multinuclear complexes. The coupling is determined by the geometry in the plane of the Cu^{II} ions, with a strong influence from the proton on the bridging hydroxido ion. As our assemblies show significant hydrogen bonding interactions, it could be that by altering the nature of these supramolecular interactions that we can tune the magnetic interaction.

Electronic Supplementary information

X-ray crystallographic data in CIF format, Chart S1, Scheme S1, Figures S1−S16, Tables S1−S4. CCDC 1828020, 1828021 and 1828022 contain the supplementary crystallographic data in CIF format for complexes **1**−**3**.

Author Information

Corresponding Author

*E-mail: dray@chem.iitkgp.ernet.in. Tel: (+91) 3222-283324. Fax: (+91) 3222-82252.

ORCID

Debashis Ray: 0000-0002-4174-6445

Conflict of interest

The authors declare no competing financial interest

Acknowledgements

M.D. is grateful to IIT Kharagpur for her research fellowship. We are also thankful to DST, New Delhi, for providing the Single Crystal X-ray Diffractometer facility in the Department of Chemistry, IIT Kharagpur under FIST program. EPR facility by CRF, IIT Kharagpur is

View Article Online
DOI: 10.1039/C8NJ02131G

duly acknowledged. M.D. is thankful to Mr. Sudipto Khamrui for his help with EPR measurements.

References

1 E. I. Solomon, D. E. Heppner, E. M. Johnston, J. W. Ginsbach, J. Cirera, M. Qayyum, M. T. Kieber-Emmons, C. H. Kjaergaard, R. G. Hadt and L. Tian, *Chem. Rev*., 2014, **114**, 3659−3853.

2 L. Casella, E. Monzani, M. Gullotti, D. Cavagnino, G. Cerina, L. Santagostini and R. Ugo, *Inorg. Chem*., 1996, **35**, 7516−7525.

3 T. W. Hambley, *Dalton Trans*., 2007, 4929−4937.

4 K. H. Thompson and C. Orvig, *Dalton Trans*., 2006, 761−764.

5 B. S. Creaven, B. Duff, D. A. Egan, K. Kavanagh, G. Rosair, V. R. Thangella and M. Walsh, *Inorg. Chim.Acta*, 2010, **363**, 4048−4058.

6 N. A. Rey, A. Neves, P. P. Silva, F. C. S. Paula, J. N. Silveira, F. V. Botelho, L. Q. Vieira, C. T. Pich, H. Terenzi and E. C. Pereira-Maia, *J. Inorg. Biochem*., 2009, **103**, 1323−1330.

7 N. A. Rey, A. Neves, A. J. Bortoluzzi, C. T. Pich and H. Terenzi, *Inorg. Chem*., 2007, **46**, 348−350.

8 M. Pait, E. Colacio and D. Ray, *Polyhedron*, 2015, **88**, 90-100.

9 A. Escuer, G. Vlahopoulou, S. P. Perlepes and F. A. Mautner, *Inorg. Chem.*, 2011, **50**, 2468–2478.

10 M. Sarkar, R. Clérac, C. Mathoniere, N. G. R. Hearns, V. Bertolasi and D. Ray, *Inorg. Chem*., 2010, **49**, 6575–6585.

11 E. Bosch and C. L. Barnes, *J. Coord. Chem.*, 2003, **56**, 329–336.

12 H. Liu, H. Wang, H. Wu and D. Niu, *J. Coord. Chem*., 2005, **58**, 1345–1349.

13 K. Chattopadhyay, B. K. Shaw, S. K. Saha and D. Ray, *Dalton Trans*., 2016, **45**, 6928−6938.

14. A. Chatterjee, H. R. Yadav, A. R. Choudhury, A. Ali, Y. Singh and R. Ghosh, *Polyhedron*, 2018, **141**, 140–146.

15. S. Tabassum, M. Afzal, H. Al-Lohedan, M. Zaki, R. A. Khan and M. Ahmad, *Inorg. Chim. Acta*, 2017, **463**, 142–155.

16 D. Mandal, M. Chauhan, F. Arjmand, G. Aromi and D. Ray, *Dalton Trans*., 2009, **42**, 9183−9191.

17 R. S. Drago, *Physical Methods in Chemistry*, W. B. Saunders Company, 2nd edn, 1965.

View Article Online
DOI: 10.1039/C8NJ02131G

18 F. S. Tiago, P. H. O. Santiago, M. M. P. Amaral, J. B. L. Martins and C. C. Gatto, *J. Coord. Chem*., 2016, **69**, 330−342.

19 N. Hussain and V. K. Bhardwaj, *Dalton Trans.*, 2016, **45**, 7697−7707.

20 K. Nakamoto, *Infrared and Raman Spectra of Inorganic and Coordination Compounds*, Wiley, New York, 4th edn, 1986.

21 D. L. Lewis, E. D. Estes and D. J. Hodgson, *J. Cryst. Mol. Struct*., 1975, **5**, 67−74.

22 G. B. Deacon, R. J. Phillips, *Coord. Chem. Rev*., 1980, **33**, 270–250.

23 A. Ozarowski, I. B. Szymanska, T. Muziol and J. Jezierska, *J. Am. Chem. Soc*., 2009, **131**, 10279−10292.

24 S. Sarkar, S. Majumder, S. Sasmal, L. Carrella, E. Rentschler and S. Mohanta, *Polyhedron*, 2013, **50**, 270–282.

25 A. T. Baker, *J. Chem. Educ*., 1998, **75**, 98–99.

26 C. V. Esteves, P. Lamosa, R. Delgado, J. Costa, P. Desogere, Y. Rousselin, C. Goze and F. Denat, *Inorg.Chem*., 2013, **52**, 5138−5153.

27 T. Ash, T. Debnath, T. Banu and A. K. Das, *J. Phys. Chem. B*., 2016, **120**, 3467−3478.

28 A. W. Addison, T. N. Rao, J. Reedijk, J. V. Rijn and G. C. Verschoor, *J. Chem. Soc.*, *Dalton Trans*., 1984, 1349–1356.

29 A. K. Ghosh, R. Clerac, C. Mathoniere and D. Ray, *Polyhedron*, 2013, **54**, 196–200.

30 J.-C. Jiang, Z.-L. Chu, W. Huang, G. Wang and X.-Z. You, *Inorg. Chem*., 2010, **49**, 5897–5911.

31 E. V. Karpova, A. I. Boltalin, M. A. Zakharov, N. I. Sorokina, Y. M. Korenev and S. I. Troyanov, *Z. Anorg. Allg. Chem*., 1998, **624**, 741–744.

32 N. Marino, A. E. Rabideau and R. P. Doyle, *Inorg. Chem*., 2011, **50**, 220–230.

33 M. F. Primik, S. Goeschl, S. M. Meier, N. Eberherr, M. A. Jakupec, E. A. Enyedy, G. Novitchi and V. B. Arion, *Inorg. Chem*., 2013, **52**, 10137−10146.

34 Y. Cui, J.-T. Chen and J.-S. Huang, *Inorg. Chim.Acta*, 1999, **293**, 129−139.

35 A. R. Paital, V. Bertolasi, G. Aromi, J. Ribas-Arino and D. Ray, *Dalton Trans*., 2008, 861−864.

36 A. Rockenbauer and L. Korecz, *Appl. Magn. Reson*., 1996, **10**, 29–43.

37 E. B. Seena and M. R. P. Kurup, *Polyhedron*, 2007, **26**, 829–836.

38 B. J. Hathaway and D. E. Billing, *Coord. Chem. Rev*., 1970, **5**, 143–207.

39 M. Joseph, M. Kuriakose, M. R. P. Kurup, E. Suresh, A. Kishore and S. G. Bhat, *Polyhedron*, 2006, **25**, 61–70.

40 J. Padilla, D. Gatteschi and P. Chaudhuri, *Inorg. Chim. Acta*, 1997, **260**, 217–220.

View Article Online
DOI: 10.1039/C8NJ02131G

41 N. F. Chilton, R. P. Anderson, L. D. Turner, A. Soncini and K. S. Murray, *J. Comput. Chem*., 2013, **34**, 1164–1175.

42 S. Roy, R. J. Butcher, M. S. El Fallah, J. Tercero and J. C. Pessoa, *Polyhdron*, 2013, **53**, 269–277.

43 E. Ruiz, P. Alemany, S. Alvarez and J. Cano, *J. Am. Chem. Soc*., 1997, **119**, 1297–1303.

44 E. Ruiz, P. Alemany, S. Alvarez and J. Cano, *Inorg. Chem*., 1997, **36**, 3683–3688.

45 R. R. Gagne, C. L. Spiro, T. J. Smith, C. A. Hamann, W. R. Thies and A. D. Shiemke, *J. Am. Chem. Soc.*, 1981, **103**, 4073−4081.

46 *Saint, Smart and XPREP*, Siemens Analytical X-ray Instruments Inc., Madison, WI, 1995.

47 G. M. Sheldrick, *SHELXS-2014*, *Program for Crystal Structure Solution*, University of Göttingen, 2014.

48 G. M. Sheldrick, *Crystal structure refinement with SHELXL*. *Acta Crystallogr.,Sect. A: Found. Crystallogr*., 2008, **64**, 112−122.

49 L. Farrugia, *WinGX-Version 2014.1*, *J. Appl. Crystallogr*., 2012, **45**, 849−854.

50 G. M. Sheldrick, *SADABS Software for Empirical Absorption Correction*, University of Göttingen, Institute fur Anorganische Chemieder Universitat, Göttingen, Germany, 1999−2003.

51 *DIAMOND, Visual Crystal Structure Information System*, *version 3.1*, Crystal Impact, Bonn, Germany, 2004.

52 M. J. Frisch, G. W. Trucks, H. B. Schlegel, G. E. Scuseria, M. A. Robb, J. R. Cheeseman, G. Scalmani, V. Barone, B. Mennucci, G. A. Petersson, H. Nakatsuji, M. Caricato, X. Li, H. P. Hratchian, A. F. Izmaylov, J. Bloino, G. Zheng, J. L. Sonnenberg, M. Hada, M. Ehara, K. Toyota, R. Fukuda, J. Hasegawa, M. Ishida, T. Nakajima, Y. Honda, O. Kitao, H. Nakai, T. Vreven, J. A. Montgomery, Jr., J. E. Peralta, F. Ogliaro, M. Bearpark, J. J. Heyd, E. Brothers, K. N. Kudin, V. N. Staroverov, R. Kobayashi, J. Normand, K. Raghavachari, A. Rendell, J. C. Burant, S. S. Iyengar, J. Tomasi, M. Cossi, N. Rega, J. M. Millam, M. Klene, J. E. Knox, J. B. Cross, V. Bakken, C. Adamo, J. Jaramillo, R. Gomperts, R. E. Stratmann, O. Yazyev, A. J. Austin, R. Cammi, C. Pomelli, J. W. Ochterski, R. L. Martin, K. Morokuma, V. G. Zakrzewski, G. A. Voth, P. Salvador, J. J. Dannenberg, S. Dapprich, A. D. Daniels, Ö. Farkas, J. B. Foresman, J. V. Ortiz, J. Cioslowski and D. J. Fox, Gaussian 09, Revision D.01; Gaussian, Inc.: Wallingford, CT, 2009.

53 L. Noodleman, *J. Chem. Phys*., 1981, **74**, 5737– 5743.

54 L. Noodleman and E. R. Davidson, *Chem. Phys*., 1986, **109**, 131– 143.

View Article Online
DOI: 10.1039/C8NJ02131G

55 L. Noodleman, C. Y. Peng, D. A. Case and J.-M. Mouesca, *Coord. Chem. Rev*., 1995, **144**, 199– 244.

56 A. D. Becke, *J. Chem. Phys*., 1993, **98**, 5648–5652.

57 R. Ditchfield, W. J. Hehre and J. A. Pople, *J. Chem. Phys*., 1971, **54**, 724–728.

58 E. Ruiz, A. Rodríguez-Fortea, J. Cano, S. Alvarez and P. Alemany, *J. Comput. Chem*., 2003, **24**, 982–989.

59 E. Ruiz, S. Alvarez, J. Cano and V. Polo, *J. Chem. Phys*., 2005, **123**, 164110– 164117.

View Article Online
DOI: 10.1039/C8NJ02131G

Table of Contents

Family of $[Cu_2]$, $[Cu_4]$ and $[Cu_5]$ Aggregates: Alteration of Reaction Conditions, Ancillary Bridges and Capping Anions

Manisha Das,[a] Gavin A. Craig,[b] Daniel Escudero,[c] Mark Murrie,[b] Antonio Frontera,[d] and Debashis Ray*[,a]

Enforced coordination by NO_3^-, ClO_4^- and CF_3COO^- groups resulted in $[Cu_2]$ (**1**), $[Cu_4]$ (**2**) and $[Cu_5]$ (**3**) complexes using H_5L1.